Impulsive Multivariate Interference Models for IoT Networks

Ce Zheng, Malcolm Egan, Laurent Clavier, Gareth W. Peters, Jean-Marie Gorce

Impulsive Multivariate Interference Models for IoT Networks

Ce Zheng, Malcolm Egan, Laurent Clavier, Gareth W. Peters and Jean-Marie Gorce

***Abstract*—Device density in wireless internet of things (IoT) networks is now rapidly increasing and is expected to continue in the coming years. As a consequence, interference is a crucial limiting factor on network performance. This is true for all protocols operating on ISM bands (such as SigFox and LoRa) and licensed bands (such as NB-IoT). In this paper, with the aim of improving system design, we study the statistics of the interference due to devices in IoT networks; particularly those exploiting NB-IoT. Existing theoretical and experimental works have suggested that interference on each subband is well-modeled by impulsive noise, such as α-stable noise. If these devices operate on multiple partially overlapping resource blocks—which is an option standardized in NB-IoT—complex statistical dependence between interference on each subband is introduced. To characterize the multivariate statistics of interference on multiple subbands, we develop a new model based on copula theory and demonstrate that it effectively captures both the marginal α-stable model and the dependence structure induced by overlapping resource blocks. We also develop a low complexity estimation procedure tailored to our interference model, which means that the copula model can often be expressed in terms of standard network parameters without significant delays for calibration. We then apply our interference model in order to optimize receiver design, which provides a tractable means of outperforming existing methods for a wide range of network parameters.**

I. Introduction

With the increasing scale of wireless network deployments for the Internet of Things (IoT), an ongoing question is to ensure that these networks meet reliability and latency requirements. A difficulty in network design is that interference from a large number of devices, even if they operate at low power levels, can significantly degrade the performance of other nearby wireless communication networks.

A key protocol for IoT communications is Narrowband IoT (NB-IoT) [2]–[4]. Due to the small quantities of data that IoT devices are typically required to transmit, a standard setting is to restrict IoT devices to use a single subband. In this case, the baseband interference vector consisting of the interference on each subband has statistically independent components.

Under the assumption of IoT device locations governed by a homogeneous Poisson point process or a doubly Poisson cluster process, the interference on a single subband has been extensively studied. In particular, it is known that both the power and amplitude of the interference are heavy-tailed, often well approximated by α-stable statistics [5]–[10]. Moreover, recent experiments on the 868 MHz band in Aalborg have suggested that the interference power is heavy-tailed, consistent with α-stable models [11]–[13].

Under the homogeneous Poisson point process model for device locations, there is now an extensive body of work on performance analysis for transmissions on a single subband. In [7], the uncoded probability of error has been characterized. The outage probability and ergodic rate have been largely studied via Laplace transform-type methods exploiting tools such as the probability generating functional [14]–[16]. However, this existing analysis assumes that the locations of the interferers do not change rapidly, called the slowly varying case by Pinto and Win [7], [8].

When interferers change rapidly—the fast varying case—a more suitable model is the memoryless additive α-stable noise channel [17]. The capacity of this channel has been studied in [18], [19], where tight upper and lower bounds have been established under generalized power constraints, and in [20], [21] where the structure of the optimal input distribution has been investigated. A key observation is that to study the fast varying case, a characterization of the interference statistics must be explicitly obtained, rather than implicitly as in the Laplace transform-based methods.

Little is known about the interference statistics nor system performance when transmissions utilize multiple subbands. In [22], [23], optimal linear combiners were obtained for statistically independent interference on each subband. The general case with non-trivial dependence arises when each IoT device can simultaneously access multiple subbands. In this setting, the only characterization and analysis is given in [24] for linear combining, where a Gaussian assumption on the combination of the fading and baseband emission statistics is required.

A characterization of the general multivariate dependence structures for the interference is relevant for NB-IoT with 15 kHz bandwidth spacing, which allows each device to access up to 12 subbands [2]. Beyond existing standardized protocols for the NB-IoT, advanced non-orthogonal multiple access (NOMA) techniques such as sparse code multiple access (SCMA) [25] require that each device is capable of utilizing multiple subbands. Such approaches can facilitate coding over both time and frequency, leading to reduced latencies by requiring fewer OFDM symbols per transmission. This is expected to be critical for real-time applications relying on low latency communications.

In this paper, motivated by the existing NB-IoT protocol and proposed NOMA schemes, we study the multivariate interference statistics where each device can simultaneous-

Elements of this work appeared in the 2019 IEEE International Conference on Communications (ICC) [1] C. Zheng and L. Clavier are with Université de Lille 1, IEMN UMR CNRS 8520, IRCICA USR CNRS 3380, Villeneuve d'Ascq, France. M. Egan and J.-M. Gorce are with Univ. Lyon, INSA Lyon, INRIA, CITI, France. L. Clavier is also with IMT Lille Douai, France. G.W. Peters is with the School of Mathematical and Computer Sciences, Heriot-Watt University, UK.

ly access multiple subbands. We consider devices located according to both homogeneous Poisson point process, as well as the doubly Poisson cluster process and Matérn hard-core process of type II, which can capture attraction and repulsion. These general families of point processes are able to account for clustering due to human activity in certain regions, such as smart home devices or e-health devices in hospitals. On the other hand, devices exploiting carrier-sense multiple access with collision avoidance (CSMA/MA) induces device locations better modeled by Matérn hard-core processes [26].

We first establish that the α-stable model forms a good approximation for the interference on each subband. While such an approximation has long been known for interference induced by device locations governed by homogeneous Poisson point process, it has not been justified for more general point process models. The main exception is [9], which considers a particular doubly Poisson cluster model and does not examine the feasibility of the α-stable approximation for general parameter choices.

We validate the α-stable approximation on a single subband by first observing that each of the more general families of point processes induces interference that converges in distribution to interference induced by a homogeneous Poisson point process. We then verify via simulation that the Kullback-Leibler (KL) divergence between the α-stable interference model and the interference arising from the general point process models is indeed small for practical parameter choices.

The key challenge is then to characterize the multivariate interference distribution, given the marginals are known to be well-approximated by the α-stable distribution. We show that in the limiting case, where all devices transmit on all subbands, the interference forms a sub-Gaussian α-stable random vector. For devices with a low probability of transmission, we show that the interference can be well-modeled by blocks of independent low dimensional sub-Gaussian α-stable random vectors. In more general scenarios, the joint distribution is not tractable and cannot be characterized directly. To this end, we propose a new model based on the t-copula. This approach has the advantage of leading to a tractable joint distribution with a small number of parameters.

We then focus on parameter estimation for the t-copula model. While there exist methods to approximate the maximum likelihood estimate for the t-copula parameters, these can require a large number of interference samples. Instead—for the particular distributions arising from interference—we obtain a closed-form estimate depending on the parameters of the marginal distributions. We show that the resulting model agrees well with the true interference distribution (obtained via simulation) in terms of the KL divergence for a range of service rates.

To apply our new interference models, we focus on receiver design to detect binary signals in the presence of multivariate IoT interference. By designing receivers based on our interference models there is a significant improvement in the probability of error compared with maximal ratio combining and standard methods tailored to α-stable noise [22], [23].

The remainder of this paper is organized as follows: Section II describes the system model. Section III characterizes the multivariate impulsive interference when interferers are located according to a homogeneous Poisson point process, a doubly Poisson cluster process or a Matérn hard-core process of type II. Section IV proposes a low complexity parameter estimation method tailored to the interference model. Section V verifies the models and the proposed estimation method. Section VI studies the impact of multivariate impulsive interference on receiver design. Section VII concludes the paper.

Notation

Vectors are denoted by bold lowercase letters and random vectors by bold uppercase letters, respectively (e.g., $\mathbf{x}$, $\mathbf{X}$). We denote the distribution of a random vector $\mathbf{X}$ by $P_{\mathbf{X}}$. If $\mathbf{X}, \mathbf{Y}$ are two random vectors equal in distribution, then we write $\mathbf{X} \stackrel{d}{=} \mathbf{Y}$.

Let $\mathbf{X}$ and $\mathbf{Y}$ be continuous random vectors on $\mathbb{R}^d$ with distributions $P_{\mathbf{X}}$ and $P_{\mathbf{Y}}$, respectively. The density of $\mathbf{X}$ is denoted by $p_{\mathbf{X}}$ and the density of $\mathbf{Y}$ by $p_{\mathbf{Y}}$. Then, the Kullback-Leibler (KL) divergence between $\mathbf{X}$ and $\mathbf{Y}$ is defined by

$$D_{KL}(P_{\mathbf{X}}||P_{\mathbf{Y}}) = \int_{\mathbb{R}^d} p_{\mathbf{X}}(\mathbf{x}) \log \frac{p_{\mathbf{X}}(\mathbf{x})}{p_{\mathbf{Y}}(\mathbf{x})} d\mathbf{x}. \tag{1}$$

Let $f : \mathbb{R} \to \mathbb{R}$ and $g : \mathbb{R} \to \mathbb{R}$. We use the Landau notation where $f(x) = o(g(x))$ if $\lim_{x\to\infty} \frac{f(x)}{g(x)} = 0$.

II. System Model

Consider a network of devices located according to a general point process, denoted by Φ. These devices form interferers for a receiver located at the origin. We focus on three models for Φ (precise definitions can be found in [27]):

(i) *Homogeneous Poisson point process* with intensity λ devices$/m^2$;

(ii) *Doubly Poisson cluster process*: the parent point process is a homogeneous Poisson point process with intensity λ_p devices$/m^2$, and each daughter process, centered on its parent's position, is also a homogeneous Poisson point process with intensity λ_d devices$/m^2$ restricted to a disc of radius r_c. Points from the parent homogeneous Poisson point process are included.[1] Hence, the average number of points in each cluster is $c = \lambda_d \pi r_c^2 + 1$ devices.

(iii) *Matérn hard-core process of type II*: the underlying homogeneous Poisson point process is with intensity λ_p devices$/m^2$, and the hard-core distance is r_h.

These three point processes are representative of a large family of processes in that the homogeneous Poisson point process exhibits uniform behavior in the sense that conditioned on the number of points in a region, each point is uniformly and independently distributed in the region. On the other hand, the doubly Poisson cluster process exhibits attraction, while the Matérn hard-core process of type II exhibits repulsion. We remark that these models can capture the activity of devices

[1]We remark that a standard formulation of the doubly Poisson cluster process studied in [9], known as the Neyman-Scott process, does not include the parent process points. However, doing so does not significantly change the interference statistics and enables the rigorous approximation theorems in Section III.

under both duty cycle constraints and, in the case of the Matérn hard-core process, CSMA-type protocols [26].

In each case, the intensity—e.g., λ in the case of the homogeneous Poisson point process—corresponds to the intensity of active devices with data to transmit. In 5G, a common target is one device per square meter; however, the density of active devices with a given protocol, in a given time-frame and spectrum band, may be significantly lower. We will often set $\lambda \in [0.001, 0.01]$ devices$/m^2$.

Physical considerations require that the radius of the network, $r_{\max}$, is finite and that there is a minimum distance between the receiver and the closest interferer, $r_{\min}$. To this end, define the annulus

$$\Gamma(r_{\min}, r_{\max}) = \{\mathbf{x} \in \mathbb{R}^2 : r_{\min} \leq \|\mathbf{x}\| \leq r_{\max}\}. \quad (2)$$

Restricting Φ to this annulus yields a new point process, which is denoted by

$$\Phi_{\Gamma(r_{\min}, r_{\max})} = \Phi \cap \Gamma(r_{\min}, r_{\max}). \quad (3)$$

We assume that a frequency band is shared by the devices in $\Phi_{\Gamma(r_{\min}, r_{\max})}$ and completely observed by the receiver at the origin. For example, the frequency band might correspond to the $863-870$ MHz bands used for low power wide area networks [11]. This frequency band is divided into K blocks, denoted by $\mathcal{B} = \{B_1, \ldots, B_K\}$. Moreover, each block contains N subbands; that is, each $B_u = \{b_{u,1}, \ldots, b_{u,N}\}$, $u = 1, \ldots, K$. This setup is illustrated in Fig. 1, where there are $K = 6$ blocks and each block contains $N = 3$ subbands.

Remark 1. *In the NB-IoT protocol for uplink transmissions (NB-PUSCH), each block can contain $N = 1, 3, 6, 12$ subbands with a 15 kHz spacing [2]. Nevertheless, we carry out a more general analysis as future protocols (e.g., SCMA) may allow a larger choice of subbands per block.*

When a device transmits using the frequency block B_u, all subbands $b_{u,1}, \ldots, b_{u,N}$ are utilized. Moreover, the subbands in B_u are disjoint from the subbands in any other block $B_{u'}$ for $u' \neq u$. In a given time-slot, each interfering device transmits on a set of frequency blocks in $\mathcal{B}$. In particular, the interfering device scans all frequency blocks in $\mathcal{B}$, selecting each block B_u in $\mathcal{B}$ randomly and independently with probability p. As a consequence, the probability that a given device transmits on k blocks in $\mathcal{B}$ is given by $\binom{K}{k} p^k (1-p)^{K-k}$. We also assume that each of the blocks selected by any device $k \in \Phi_{\Gamma(r_{\min}, r_{\max})}$ are independent of the blocks selected by any other device k'. The set of devices transmitting on block B_u is denoted by Φ_{B_u}.

The access probability p can be interpreted in terms of a service rate; that is, the average quantity of data that each device is required to transmit. Note that when each device is required to transmit a large quantity of data, p will be larger. In this work, we assume that p is the same for each device. We identify three scenarios: heavily loaded networks, corresponding to $p \approx 1$; moderately loaded networks, corresponding to $0 < p < 1$; and lightly loaded networks, corresponding to $p \approx 0$. We remark that the most common variant of the NB-IoT protocol can be well approximated for small $p > 0$, where (with high probability) only a single subband is utilized. However as detailed in Remark 1, even in NB-IoT multiple subbands may be utilized per device.

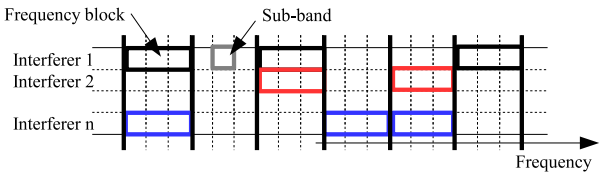

Fig. 1. Illustration of the model with $K = 6$ frequency blocks, each containing $N = 3$ subbands.

Consider a subband $i \in \{1, \ldots, N\}$ associated with the block B_u. The interference observed by the receiver at the origin on this subband is given by

$$Z_{B_{u,i}} = \sum_{j \in \Phi_{B_u}} r_j^{-\frac{\eta}{2}} h_{j,i} x_{j,i}, \quad (4)$$

where r_j is the distance from device j to the origin, $\eta > 2$ is the path-loss exponent, $h_{j,i}$ is the fading coefficient for device j on subband i, and $x_{j,i}$ is the baseband emission.

After stacking the interference on each subband for each block, the resulting interference random vector is given by

$$\mathbf{Z} = \left[\mathrm{Re}(Z_{b_{1,1}}), \mathrm{Im}(Z_{b_{1,1}}), \ldots, \mathrm{Re}(Z_{b_{K,N}}), \mathrm{Im}(Z_{b_{K,N}})\right]^T. \quad (5)$$

The study of the interference random vector $\mathbf{Z}$ is the focus of this paper. It is known that under the assumptions in this section, each pair $(\mathrm{Re}(Z_{B_{u,i}}), \mathrm{Im}(Z_{B_{u,i}}))$ has a log-characteristic function given in [9, Eq. (13)]. However, this representation is not amenable to the study of the random vector $\mathbf{Z}$ in (5). As such, we investigate alternative approximations of the marginal distributions in the following section.

III. Interference Characterization

In this section, we obtain an exact characterization or a good approximation of the joint distribution for the interference random vector in (5) for each of the three point processes governing device locations. We first establish a general convergence result, relating interference induced by limiting cases of doubly Poisson cluster processes and Matérn hard-core processes of type II to interference induced by homogeneous Poisson point processes. This provides a means of obtaining a unified characterization for the interference distribution arising from each point process. We then study in detail the interference random vector arising from the homogeneous Poisson point process model.

The main results in this section are the following: *(a)* the interference on a single subband is well approximated as an isotropic α-stable random variable; *(b)* the interference vector is a sub-Gaussian α-stable random vector if the set of interferers on each subband are the same, i.e., p=1; *(c)* the more general case of partially overlapping interferers can be modeled via a t-copula and α-stable marginals.

Statistical models based on α-stable random vectors are used extensively. Background material on these models is provided in Appendix A along with references for further details.

A. Approximations of the Interference Distribution Induced by General Point Processes

A key feature of doubly Poisson cluster processes and Matérn hard-core processes of type II is that they are constructed from homogeneous Poisson processes. As such, it may be expected that for certain choices of parameters, the process is well approximated by a homogeneous Poisson point process. Moreover, the resulting distribution of the interference may be well approximated by the distribution of the interference arising from the homogeneous Poisson point process. In this case, the interference statistics arising from the homogeneous Poisson point process form a unifying approximation for the more general families of point processes.

In Theorem 1 we make these assertions precise. We establish that under a range of fading models, the interference induced by $\Phi_{\Gamma(r_{\min},r_{\max})}$ for the point processes in Section II converges in distribution to the interference induced by a homogeneous Poisson point process restricted to the annulus $\Gamma(r_{\min}, r_{\max})$. This is achieved by introducing a sequence of point processes parameterized by a sequence of parameters $(\kappa_n)_{n=1}^{\infty}$, which converges to a parameter κ_0 corresponding to a homogeneous Poisson point process.

To present our approximation result, let $\Phi^{\kappa_n}_{\Gamma(r_{\min},r_{\max})}$ be a doubly Poisson cluster process or a Matérn hard-core process of type II with intensity λ and parameter κ_n. In the case of the doubly Poisson cluster process, κ_n corresponds to the intensity λ_d of the daughter process, and $\kappa_0 = 0$. On the other hand, for the Matérn hard-core process of type II, κ_n corresponds to the hard-core distance c, and $\kappa_0 = 0$. We denote the interference induced by $\Phi^{\kappa_n}_{\Gamma(r_{\min},r_{\max})}$ by $\mathbf{Z}_n$, where $\mathbf{Z}_n$ corresponds to the interference random vector in (5).

Theorem 1. *Let $\Phi^{\kappa_n}_{\Gamma(r_{\min},r_{\max})}$ be a doubly Poisson cluster process or a Matérn hard-core process of type II with intensity λ and parameter κ_n such that $\kappa_0 = \lim_{n\to\infty}\kappa_n$. Suppose that $\Phi^{\kappa_0}_{\Gamma(0,\infty)}$ is a homogeneous Poisson point process with intensity λ and $\operatorname{supp}(h_{j,i}x_{j,i})$ in (4) is compact for all $i=1,\ldots,N$, $j \in \Phi^{\kappa_n}_{\Gamma(r_{\min},r_{\max})}$ and $n\in\mathbb{N}$. Then, $\mathbf{Z}_n \xrightarrow{d} \mathbf{Z}_0$ as $n \to \infty$.*

Proof. See Appendix B. □

Theorem 1 provides a justification for approximating the interference statistics induced by doubly Poisson cluster processes and Matérn hard-core processes of type II by interference from homogeneous Poisson point processes. As such, we now focus on characterizing the joint distribution arising from the homogeneous Poisson point process. In Section V, we verify via a simulation study that for practical choices of parameters, the homogeneous Point process approximation is in fact valid.

B. Subband Interference Characterization

Remark 2. *In the remainder of this section (i.e., Section III-B and Section III-C), we assume that Φ is a homogeneous Poisson point process with intensity λ, $r_{\min} = 0$ and $r_{\max} = \infty$.*

We first turn to the interference on each subband. In this case, α-stable approximations for the interference have been widely studied [5]–[7], [9]. The fundamental reason for this is due to the following theorem (given in this form in [28]).

Theorem 2. *Consider the interference on subband i of block B_u, denoted by $Z_{b_{u,i}}$ in (4). Suppose that $h_{j,i}x_{j,i}$ in (4) is an isotropic complex random variable and*

$$\mathbb{E}[|\mathrm{Re}(h_{j,i}x_{j,i})|^{4/\eta}] < \infty, \tag{6}$$

with $\eta > 2$, Then, $Z_{b_{u,i}}$ in (4) converges almost surely to an isotropic $4/\eta$-stable random variable.

Moreover, if the fading coefficients $h_{j,i}$ are i.i.d. and baseband emissions $x_{j,i}$ are also i.i.d. then the scale parameters of real and imaginary components are equal, given by

$$\sigma_{Z_{b_{u,i}}} = \left(\pi\lambda p C^{-1}_{\frac{4}{\eta}}\mathbb{E}[|\mathrm{Re}(h_{j,i}x_{j,i})|^{\frac{4}{\eta}}]\right)^{\frac{\eta}{4}}, \tag{7}$$

where

$$C_\alpha = \begin{cases} \frac{1-\alpha}{\Gamma(2-\alpha)\cos(\pi\alpha/2)}, & \text{if } \alpha \neq 1 \\ 2/\pi, & \text{if } \alpha = 1. \end{cases} \tag{8}$$

Theorem 2 provides a characterization of the marginal distributions for the interference random vector. In the following, we study the joint distribution.

C. Interference Random Vector Characterization

Let $\mathbf{Z}_{B_u}$ denote the interference on all subbands for a given block B_u; that is,

$$\mathbf{Z}_{B_u} = [\mathrm{Re}(Z_{b_{u,1}}), \mathrm{Im}(Z_{b_{u,1}}), \ldots, \mathrm{Re}(Z_{b_{u,N}}), \mathrm{Im}(Z_{b_{u,N}})]^T. \tag{9}$$

The following theorem provides a characterization of the interference random vector $\mathbf{Z}_{B_u}$. Recall that if a device transmits on an subband within a block B_u, then it transmits on all subbands in B_u so that the set of interferers remains unchanged on all subbands. In this special case, the interference random vector in (9) can be characterized exactly as shown in the following theorem.

Theorem 3. *Let $j \in \Phi_{B_u}$. Suppose that $h_{j,i} \sim \mathcal{CN}(0,1)$ (Rayleigh fading) or $x_{j,i} \sim \mathcal{CN}(0,P)$, $P > 0$ (Gaussian inputs), and that the conditions in Theorem 2 hold. Then, the interference random vector $\mathbf{Z}_{B_u}$ follows the sub-Gaussian α-stable distribution with an underlying Gaussian vector having i.i.d. $\mathcal{N}(0,\sigma^2_{\mathbf{Z}})$ components, $\alpha = 4/\eta$ and parameter*

$$\sigma_{\mathbf{Z}_{B_u}} = \left(\pi\lambda p C^{-1}_{\frac{4}{\eta}}\mathbb{E}[|\mathrm{Re}(h_{j,1}x_{j,1})|^{\frac{4}{\eta}}]\right)^{\frac{\eta}{4}}. \tag{10}$$

Proof. See Appendix C. □

We now turn to the general case, where devices may not necessarily transmit on all blocks simultaneously. In this scenario, the statistical dependence between the interference on distinct subbands is difficult to characterize. A popular approach in statistics to cope with this scenario is to exploit copulas, where the joint distribution function of a random vector in $\mathbb{R}^n$, say $\mathbf{X} = [X_1, \ldots, X_n]^T$, is given in the form

$$F(x_1, \ldots, x_n) = C(F_1(x_1), \ldots, F_n(x_n)), \tag{11}$$

where $C : [0,1]^n \to [0,1]$ is called a *copula function*, and F_i, $i = 1, \ldots, n$ are the marginal distribution functions. When both the joint and marginal distributions admit density functions (as is the case in the interference models considered

in this paper), the joint probability density function has the form

$$p_{\mathbf{X}}(x_1,\ldots,x_n) = c(F_1(x_1),\ldots,F_n(x_n))\prod_{i=1}^{n} p_{X_i}(x_i). \quad (12)$$

That is, the joint probability density function decomposes into the product of the marginal densities and another function $c : [0,1]^n \to \mathbb{R}_+$, which captures dependence between the different components of $\mathbf{X}$.

A highly desirable property of copula models is that they provide a parametric representation of the joint distribution for random vectors. In fact, by Sklar's Theorem [29], *any* joint distribution function admits a copula C. This copula is also unique if the marginal distributions are continuous, which is the case for the α-stable marginals arising in the context of interference modeling demonstrated in Theorem 2.

However, a key challenge in applying copulas is to obtain a tractable copula model; i.e., parameter estimation and simulation are computationally feasible. A good candidate for the copula to approximate the distribution of the interference random vector $\mathbf{Z}$ can be obtained from standard parametric classes of copulas; e.g., archimedean or t-copulas [29]. As we will show in the sequel, a particularly effective copula model is the t-copula, which we now detail.

Let F_v be the distribution of the univariate t-distribution, given by

$$F_v(x) = \int_{-\infty}^{x} \frac{\Gamma(\frac{v+1}{2})}{\sqrt{v\pi}\Gamma(\frac{v}{2})}\left(1+\frac{t^2}{v}\right)^{-\frac{v+1}{2}} \mathrm{d}t, \quad (13)$$

parameterized by the degree of freedom $v \in \mathbb{R}^+$. Moreover, the joint distribution $F_{v,\Sigma}$ of a n-dimensional multivariate t-distribution is given by

$$F_{v,\Sigma}(\mathbf{x}) = \int_{-\infty}^{x_1}\cdots\int_{-\infty}^{x_n} \frac{\Gamma(\frac{v+d}{2})}{\Gamma(\frac{v}{2})\sqrt{(\pi v)^d|\Sigma|}}\left(1+\frac{\mathbf{t}^T\Sigma^{-1}\mathbf{t}}{v}\right)^{-\frac{v+d}{2}} \mathrm{d}\mathbf{t}, \quad (14)$$

parameterized by the degree of freedom $v \in \mathbb{R}_{\geq 0}$ and the $n\times n$ correlation matrix Σ.

The t-copula is then defined as

$$C^t_{v,\Sigma}(\mathbf{u}) = F_{v,\Sigma}(F_v^{-1}(u_1),\ldots,F_v^{-1}(u_n))). \quad (15)$$

That is, the t-copula captures the dependence structure of a multivariate t-distribution without necessarily having t-distributed marginals. In particular, (15) can be used in (11) to construct multivariate distributions with α-stable marginals. This provides a basis to tractably model the interference random vectors arising from the system model in Section II.

Aside from well-modeling the interference distribution, t-copula models are also tractable. That is, efficient parameter estimation and simulation methods exist. In fact, as we will develop in Section IV, features of system detailed in Section II can be exploited to obtain even more efficient estimation and simulation procedures than the classical methods in [30].

IV. Parameter Estimation

To have practical models, it is essential to be able to estimate their parameters, which becomes computationally demanding in large dimensions for the general t-copula model [30]. An alternative approach is to exploit the connections between the t-copula parameters Σ, ν, Kendall's τ rank correlation and tail dependence. In this section, we use these connections in order to establish a low complexity estimation procedure tailored to the interference model.

A. Inference from the Margins

A standard approach for parameter estimation in t-copula models, known as inference from the margins, proceeds as follows. Consider a d-dimensional random vector $\mathbf{X} = [X_1,\ldots,X_d]^T$ on $\mathbb{R}^d$ governed by a t-copula with parameters Σ, ν. According to [31], the elements of Σ can be obtained via Kendall's τ rank correlation. Let $\mathbf{X}_i = [X_{i,1},\ldots,X_{i,d}]^T$, $i = 1,\ldots,n$ be n independent samples of $\mathbf{X}$. A natural estimator for Σ is then given by [30]

$$\hat{\Sigma}_{jk} = \sin\left(\frac{\pi}{2}\hat{\rho}_\tau(X_j,X_k)\right), \quad (16)$$

where

$$\hat{\rho}_\tau(X_j,X_k) = \binom{n}{2}^{-1}\sum_{1\leq i_1\leq i_2\leq n}\mathrm{sign}((X_{i_1,j}-X_{i_2,j})(X_{i_1,k}-X_{i_2,k})). \quad (17)$$

In general there are no guarantees that $\hat{\Sigma}$ is positive definite, nevertheless it is possible to apply adjustment techniques [32] to ensure positive definiteness. Having estimated Σ, the standard approach then obtains the degree of freedom ν via a maximum likelihood estimate given Σ [30].

An alternative method for estimating the degree of fredom also exists based on the tail dependence. In particular, consider a bivariate random vector (X_1, X_2) with marginal distributions F_1, F_2, respectively. Then, the (upper) tail dependence $\lambda_{\mathbf{X}}$ is defined by

$$\lambda_{\mathbf{X}} = \lim_{u\to 1}\Pr\left(X_1 > F_1^{-1}(u) | X_2 > F_2^{-1}(u)\right). \quad (18)$$

In the case that (X_1, X_2) is governed by a t-copula, [30, Proposition 1] provides a link between the tail dependence and the degree of freedom ν. For a random vector $\mathbf{X}$, if the tail dependence is known to be constant amongst each pair of elements in $\mathbf{X}$ then the degree of freedom ν can be obtained from the tail dependence $\lambda_{\mathbf{X}}$ via [30]

$$\lambda_{\mathbf{X}} = 2F_{v+1}\left(\frac{\sqrt{1+\nu}\sqrt{1-\rho}}{\sqrt{1+\rho}}\right). \quad (19)$$

where $F_{\nu+1}$ is defined in (13) with degree of freedom $\nu+1$.

B. A Low Complexity Estimation Procedure

We now develop a new low complexity estimation procedure based on a characterization of the tail dependence, detailed in Algorithm 1. This algorithm is based on a new approximation of the tail dependence in (19). To proceed, we first note that the tail dependence is not the same for each pair of elements in $\mathbf{Z}$. This is due to the fact that for a given block B_u, the random vector is sub-Gaussian α-stable. This implies that for

any pair of elements in $\mathbf{Z}_{B_u}$, the tail dependence is given by [33]

$$\lambda_{\mathbf{Z}_{B_u}} = \frac{\int_0^{\frac{1}{\sqrt{2}}} \frac{u^\alpha}{\sqrt{1-u^2}} du}{\int_0^1 \frac{u^\alpha}{\sqrt{1-u^2}} du}. \quad (20)$$

On the other hand, the tail dependence between pairs from different blocks in $\mathbf{Z}$ depends on the service rate p. For example, as $p \to 0$, elements of $\mathbf{Z}$ from different blocks are approximately independent. This means that the tail dependence for these pairs, denoted by $\lambda_{\tilde{\mathbf{Z}}}$, is approximately zero.

However, for $K > 1$, there are significantly more pairs of subbands with tail dependence $\lambda_{\tilde{\mathbf{Z}}}$ than $\lambda_{\mathbf{Z}_{B_u}}$. For this reason, we will base our estimate of the degree of freedom ν on $\lambda_{\tilde{\mathbf{Z}}}$ and verify that this approximation is accurate for sufficiently large p in Section V.

The first step is then to obtain an approximation of the tail dependence $\lambda_{\tilde{\mathbf{Z}}}$. By definition,

$$\lambda_{\tilde{\mathbf{Z}}} = \lim_{u\to 1} \Pr\left(\sum_{j\in\Phi_1} r_j^{-\frac{\eta}{2}} Z_{j,1} > F^{-1}(u) \middle| \sum_{j\in\Phi_2} r_j^{-\frac{\eta}{2}} Z_{j,2} > F^{-1}(u) \right), \quad (21)$$

By Property 1 in Appendix A, for $l \in \{1,2\}$, as $x \to \infty$

$$\Pr\left(\sum_{j\in\Phi_l} r_j^{-\frac{\eta}{2}} Z_{j,l} > x \right) = \lambda^{\frac{\eta}{4}} \mathbb{E}\left[|Z_{1,1}|^{\frac{4}{\eta}} \right] x^{-\frac{4}{\eta}} + o\left(x^{-\frac{4}{\eta}}\right). \quad (22)$$

Moreover, the dependence is also strongest between terms that have the same distance. For $p \approx 1$, this suggests the approximation

$$\Pr\left(\sum_{j\in\Phi_1} r_j^{-\frac{\eta}{2}} Z_{j,1} > F^{-1}(u), \sum_{j\in\Phi_2} r_j^{-\frac{\eta}{2}} Z_{j,2} > F^{-1}(u) \right)$$
$$\approx p \Pr\left(r_1^{-\frac{\eta}{2}} Z_{1,1} > F^{-1}(u), r_1^{-\frac{\eta}{2}} Z_{1,2} > F^{-1}(u) \right). \quad (23)$$

Since r_1 is the closest point in a homogeneous Poisson point process,

$$f_{r_1}(r) = 2p\lambda\pi r e^{-p\lambda\pi r^2}. \quad (24)$$

This yields,

$$\Pr\left(\sum_{j\in\Phi_1} r_j^{-\frac{\eta}{2}} Z_j > F^{-1}(u), \sum_{j\in\Phi_2} r_j^{-\frac{\eta}{2}} Z_j > F^{-1}(u) \right)$$
$$\approx p \int_0^\infty \left(1 - F_{Z_{1,1}}\left(\frac{F^{-1}(u)}{r_1^{-\eta/2}} \right) \right)^2 2p\lambda\pi r e^{-p\lambda\pi r^2} dr. \quad (25)$$

At this point, we make the change of variables

$$z = F^{-1}(u) r^{\frac{\eta}{2}}, \quad (26)$$

which yields (27). As such, it follows that the tail dependence is well approximated by

$$\lambda_{\tilde{\mathbf{Z}}} \approx \frac{p}{\pi\lambda \mathbb{E}\left[|\mathrm{Re}(h_{j,i} x_{j,i})|^\alpha \right]} \int_0^\infty (1 - F_{Z_{1,1}}(z))^2 \alpha z^{\alpha-1} dz \quad (28)$$

where $\alpha = 4/\eta$.

Note that the validity of swapping the limit and integral can be readily justified by an application of the dominated convergence theorem.

A key observation is that the approximation of $\lambda_{\tilde{\mathbf{Z}}}$ in (28) scales linearly with p with a maximum value corresponding to $p = 1$, which is the sub-Gaussian α-stable scenario by Theorem 3. In this case, the tail-dependence is given by

$$\lambda_{\tilde{\mathbf{Z}}} \approx \frac{1}{\pi\lambda \mathbb{E}\left[|\mathrm{Re}(h_{j,i} x_{j,i})|^{\frac{4}{\eta}} \right]} \int_0^\infty (1 - F_{Z_{1,1}}(z))^2 \frac{4}{\eta} z^{\frac{4}{\eta}-1} dz \quad (29)$$

To verify the approximation in (29), we consider the case $p = 1$. By Theorem 3, the interference random vector is sub-Gaussian α-stable. As a consequence, the tail dependence is given by (20). Fig. 2 shows that the approximation in (29) is in good agreement with the exact expression, even as α is varied. A more detailed study of the validity of the approximation is carried out in Section V. In particular, the quality of the estimation procedure is evaluated in terms of the KL divergence between the resulting interference model and the system model in Section II for the three families of point processes.

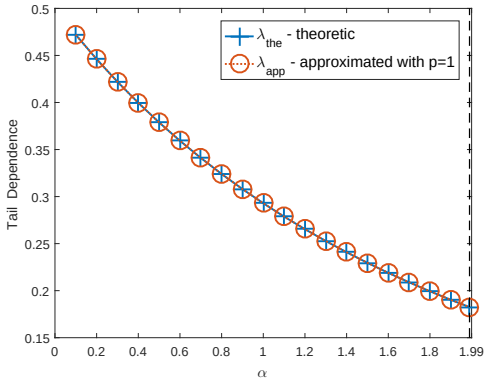

Fig. 2. Theoretical and estimated tail dependence for varying α.

Algorithm 1 Proposed Copula Parameter Estimation Algorithm with $\alpha = 4/\eta$

Input: S independent samples of the interference random vector $\mathbf{Z}^1, \ldots, \mathbf{Z}^S$.

1: Estimate the parameters of the α-stable marginals, α, γ.
2: Set the correlation matrix for the t-copula model $\Sigma = \mathbf{I}_{2KN}$.
3: Set the tail dependence for the t-copula model to be $\lambda_{\tilde{\mathbf{Z}}}$ in (28).
4: Compute the degree of freedom for the t-copula model via (19).

V. Model Verification

In this section, we compare the interference models developed in Section III with the interference arising from the scenarios detailed in Section II based on the KL divergence. We also study the dependence structure of our model and the

$$\Pr\left(\sum_{j\in\Phi_1} r_j^{-\frac{\eta}{2}} Z_j > F^{-1}(u), \sum_{j\in\Phi_2} r_j^{-\frac{\eta}{2}} Z_j > F^{-1}(u)\right) \approx p\int_0^\infty (1-F_{Z_{1,1}}(z))^2 z^{\frac{2}{\eta}} F^{-1}(u)^{-\frac{2}{\eta}} e^{-p\lambda\pi F^{-1}(u)^{-\frac{4}{\eta}} z^{\frac{4}{\eta}}} z^{\frac{4}{\eta}} F^{-1}(u)^{-\frac{2}{\eta}} \frac{2}{\eta} z^{\frac{2}{\eta}-1} dz \quad (27)$$

simulated data set via transformation to the *copula space*. This provides additional insights into the behavior of the interference, particularly when multiple subbands experience large amplitude interference.

In order to perform the model evaluation, it is necessary to calibrate and simulate the t-copula model. The α-stable parameters were obtained using the stablefit MATLAB package [34]. The t-copula parameters were then estimated using the copulafit MATLAB package [35]. Simulation methods for t-copula models are detailed in [30].

A. Interference on a Single Subband

We first verify that an α-stable model is accurate for homogeneous Poisson point processes with non-zero guard-zones as well as for the doubly Poisson cluster process and the Matérn hard-core process of type II. Fig. 3 plots a realization of the three point processes considered in this paper: homogeneous Poisson point process; doubly Poisson cluster process; and Matérn hard-core process of type II.

Theorem 2 in Section II and the approximation theorem in Section III-A suggest that the α-stable distribution is a good approximation for interference induced by homogeneous Poisson point processes, doubly Poisson cluster processes and Matérn hard-core processes of type II restricted to a finite annulus. In the sequel, we validate this approximation in terms of KL divergence through simulations.

1) Homogeneous Poisson Point Process: Consider a set of interferers governed by the point process $\Phi_{\Gamma(r_{\min},500)}$ with path loss exponent $\eta = 5$, where Φ is a homogeneous Poisson point process with intensity $\lambda = 0.001$ devices$/m^2$. Fig. 4(a) plots the impact of varying $r_{\min}$ on the KL divergence between the simulated interference in the second scenario (finite $r_{\min}$ and $r_{\max}$) and three different models: the α-stable model that assumes no guard zone (theoretical stable); an α-stable model with parameters estimated from a set of simulated data; and a fitted Gaussian model.

Observe that for a very small guard zone, the theoretical model exhibits a good fit while for a large guard zone ($r_{min} > 15$ m in our set-up) the Gaussian model is a good fit. However, in-between, the α-stable approach but with a fitted α, yields a low KL divergence, while the others do not. Variation in the parameter for the fitted α-stable model is shown in Fig. 4(b). The parameter α with the lowest KL divergence increases from approximately 0.8 (expected from the α-stable approximation since $0.8 = 4/\eta$) to nearly 2 as $r_{\min}$ ranges from 0.5 m to 50 m. Fitted α-stable models are robust to changes in $r_{\min}$—implying that the techniques in this paper hold rather generally—with the qualification that the best choice of α may be larger than $4/\eta$ as predicted by Theorem 2.

2) Doubly Poisson Cluster Process: Fig. 5(a) and Fig. 5(b) plot the impact of varying the guard-zone radius $r_{\min}$, and the

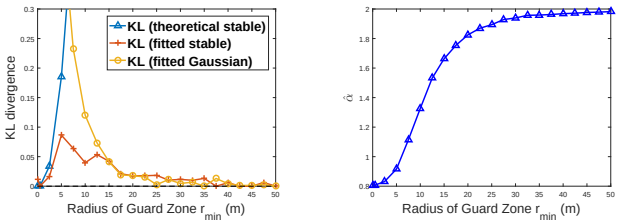

(a) Plot of the KL divergence between the simulated data set from homogeneous Poisson point process and three statistical models: theoretical stable model ($\alpha = 4/\eta$); fitted stable model ($\hat{\alpha}$); and fitted Gaussian model.

(b) Fitted stable parameter – $\hat{\alpha}$ under different $r_{\min}$ in homogeneous Poisson point processes.

Fig. 4. Homogeneous Poisson point process under different guard-zone radius

cluster radius r_c with parameters $\lambda_p = 2\times10^{-4}$ devices$/m^2$, $c = 11$ and $\eta = 3$. Since the doubly Poisson cluster process converges to the homogeneous Poisson point process as the daughter cluster intensity tends to zero, the interference with small r_c has similar behavior to that illustrated in Fig. 4(a). However, with an increase of the cluster radius r_c, the α-stable interference model approximation has a large KL divergence in the range $2.5 \le r_{\min} \le 20$ and the accuracy of the model has to be questioned. Nevertheless, as expected from Theorem 1, the α-stable model remains valid for small values of r_c and $r_{\min}$. Fig. 5(b) also verifies that the α-stable model is valid for a sufficiently small cluster radius, consistent with Theorem 1.

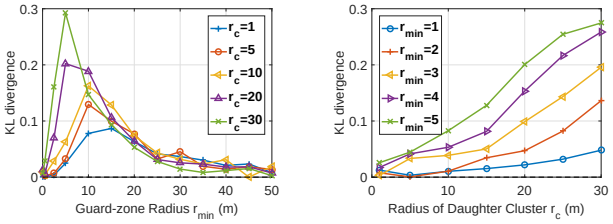

(a) Different cluster radius r_c.

(b) Different guard zone radius $r_{\min}$.

Fig. 5. Plot of the KL divergence between the simulated data set from Doubly Poisson Cluster and fitted stable model with $\hat{\alpha}$.

3) Matérn Hard-core Process of Type II: Fig. 6(a) plots the impact of varying $r_{\min}$ in the case of a Matérn hard-core process of type II under different hard-core radius r_h with parameters $\lambda_p = 0.002$ devices$/m^2$ and $\eta = 3$. Observe that unlike the doubly Poisson cluster process, the fitted α-stable model is robust to changes in $r_{\min}$. In Fig. 6(b), the impact of the hardcore radius, r_h, is illustrated. Observe that for a wide range of r_h, the KL divergence remains uniformly small.

B. Interference Random Vector: KL Divergence

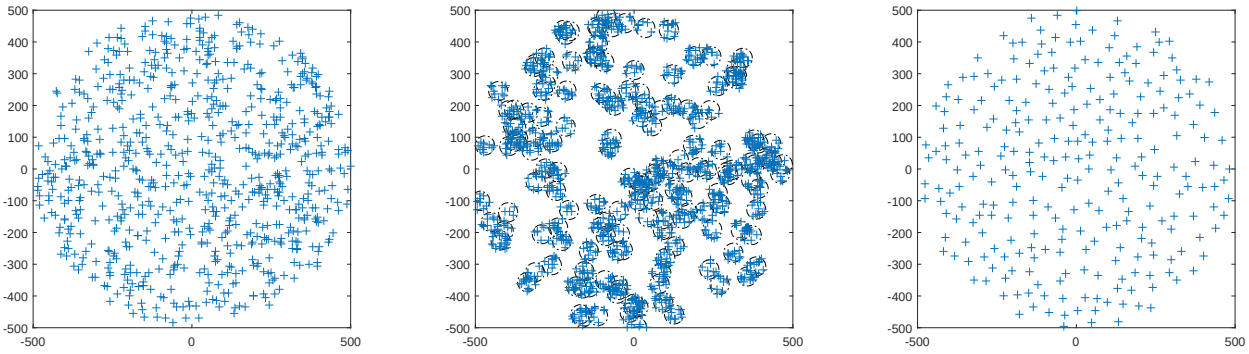

(a) Homogeneous Poisson Point Process (b) Doubly Poisson Cluster Process (c) Matérn Hard-core Process of Type II

Fig. 3. Snap shots of three point processes

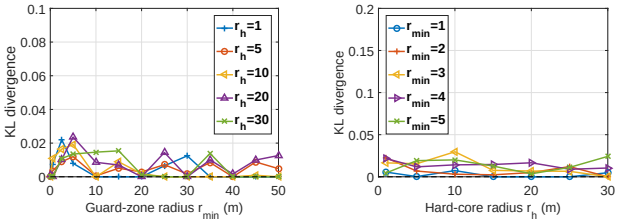

(a) Different hard-core radius r_h. (b) Different guard-zone radius $r_{\min}$.

Fig. 6. Plot of the KL divergence between the simulated data set from Matérn hard-core process of type II and fitted stable model with $\hat{\alpha}$.

We now turn to our model for the interference random vector developed in Section III-C. We numerically investigate the behavior of our proposed models by evaluating the KL divergence between the interference arising from the scenario in Section II and our models in Section III-C. That is, we estimate $D_{KL}(P||Q)$ where P is the distribution corresponding to the system model and Q is the distribution arising from our models. The interference random vector has in general a high dimension ($2KN$ dimensions for K blocks and N subbands in each block as detailed in Section II). As such, even the numerical evaluation is non-trivial and we use the k-nearest neighbor method [36] implemented in the MATLAB package [37] for computation of the KL divergence.

All figures are generated using a simulated data set with $80,000$ samples. Due to the high dimension of the interference random vector, the k-nearest neighbor method can output very small negative values [36]. In the figures, these negative values are rounded to zero.

In the experiments, we compare five models all with α-stable marginal distributions motivated by Theorem 3:

1) The t-copula α-stable model detailed in Section III-C with three different parameter estimation algorithms: *a).* via maximum likelihood estimation; *b).* via Algorithm 1 *c).* via the low complexity estimation procedure for t-copula parameters as Algorithm 1 while using the estimated $\hat{\alpha}$ in (28).
2) The independent sub-Gaussian α-stable model consisting of independent four-dimensional sub-Gaussian α-stable random vectors. In this model, the $2KN$-dimensional random interference vector $\mathbf{Z}$ is decomposed into K $2N$-dimensional random vectors (corresponding to the real and imaginary parts of two subbands on each block). Each $2N$-dimensional random vector is sub-Gaussian α-stable (see Definition 2), independent from each of the other $K-1$ two-dimensional random vectors. This model is exact when interfering devices only transmit on a single subband, the guard-zone radius $r_{\min}=0$, and the network radius $r_{\max}\to\infty$.
3) The $2KN$ sub-Gaussian α-stable model consisting of a $2KN$-dimensional sub-Gaussian α-stable random vector. This model corresponds to the scenario where all devices transmit on every block in $\mathcal{B}$, i.e., $p=1$ (see Theorem 3).

1) Homogeneous Poisson Point Process: Fig. 7(a) plots the KL divergence between the simulated data set based on the setup in Section II with $K=4$ blocks and $N=2$ subbands in each block, and the three proposed interference models. We also set $\eta=3$, $h\sim\mathcal{CN}(0,1)$, $\lambda=0.001$ devices/m^2, and $x_{j,i}$ is uniformly drawn from $\{-1,1\}$ $\forall i,j$. Observe that the $2KN$ sub-Gaussian α-stable model is in good agreement with the simulated data set as $p\to 1$. This is consistent with the characterization in Theorem 3 as when $p\to 1$ all devices transmit on all subbands with high probability. On the other hand as p decreases, the $2KN$ sub-Gaussian α-stable model is a poor fit for the simulated data set.

Fig. 7(a) also shows that the t-copula model is a good fit for a much larger range of p than the $2KN$ sub-Gaussian α-stable model. As such, it is a good choice for medium to heavily loaded IoT networks. However, for small p the t-copula model is not satisfactory.

In the lightly loaded scenario where $p\to 0$, each device transmits on more than one block with a very low probability. By the independent thinning theorem for homogeneous Poisson point processes, it then follows that the interference on each block is independent. As a consequence, the independent sub-Gaussian α-stable model is a good choice in the lightly loaded scenario. This observation is verified in Fig. 7(a), where the KL divergence for this model is nearly zero for small values of p.

2) Doubly Poisson Cluster Process: Fig. 7(b) plots the KL divergence for each of the proposed models for locations

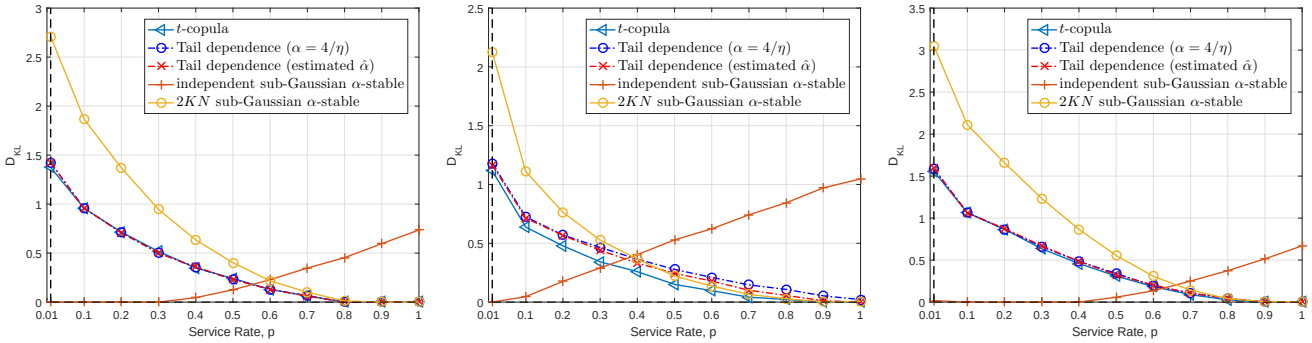

(a) Homogeneous Poisson Point Process (b) Doubly Poisson Cluster Process (c) Matérn Hard-core Process of Type II

Fig. 7. Plot of the KL divergence between the simulated data set and three statistical models: t-copula model; independent sub-Gaussian α-stable model; and $4K$ sub-Gaussian α-stable model. In the figure, $K = 4$ blocks and $N = 2$ subbands in each block are considered.

governed by a doubly Poisson cluster process with parameters: $\eta = 3$; $h \sim \mathcal{CN}(0,1)$; $\lambda = 2 \times 10^{-4}$ devices$/m^2$; $r = 30m$; $c = 11$; $x_{j,i}$ is uniformly drawn from $\{-1, 1\}$ $\forall i, j$; $K = 4$; and $N = 2$.

Observe that the t-copula model has a very similar behavior qualitatively consistent with the homogeneous Poisson point process case in Fig. 7(a). However, the low complexity estimation algorithm in Algorithm 1 has reduced performance. This is due to the implicit assumption in the estimation procedure that the void probability is that of a homogeneous Poisson point process.

3) Matérn Hard-core Process of Type II: Fig. 7(c) plots the KL divergence for each of the proposed models for locations governed by a Matérn hard-core process of type II, with parameters: $\eta = 3$; $h \sim \mathcal{CN}(0,1)$; $\lambda = 0.001$ devices$/m^2$; $r_h = 20m$; $c = 11$; $x_{j,i}$ is uniformly drawn from $\{-1, 1\}$ $\forall i, j$; $K = 4$; and $N = 2$.

Observe that the five models have the same performance in terms of KL divergence as under the homogeneous Poisson point process. This is consistent with Theorem 1 and previous work establishing that the Matérn hard-core process of type II can be well-approximated by a homogeneous Poisson point process [38], [39]. Under the Matérn hard-core process of type II, at most one point is kept within the hard-core distance based on its underlying homogeneous Poisson point process distribution. Unlike the doubly Poisson cluster process, the distribution of the closest interferer can also be approximated by (24) as shown in [40, Lemma 1]. As such, the low complexity estimation procedure in Algorithm 1 yields an estimate that well approximates the maximum likelihood estimate.

C. Interference Random Vector: Copula-Space Representations

In Section V-A, we verified that the α-stable model for the marginals is accurate for sufficiently small guard-zones and a large network radius. Using copula methods, it is also possible to qualitatively verify that the dependence structure of our multivariate interference model is also consistent. This is achieved by transforming the d-dimensional simulated data into the *copula space*, which yields a random vector on $[0,1]^d$. In particular, for both the data simulated from the system detailed in Section III-C and our copula model developed in Section III-C, we apply the transformation

$$\mathbf{Z} \mapsto [H_{\alpha,\gamma}(Z_1), \ldots, H_{\alpha,\gamma}(Z_d)]^T. \tag{30}$$

where $H_{\alpha,\gamma}(Z_i)$ is distribution function of the α-stable random variable Z_i with α and γ.

Intuitively, the copula space representation only gives information about the dependence structure, independent of the choice of the marginal distributions.

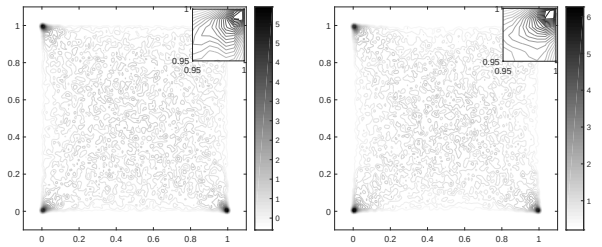

(a) Scenario based on Sec. II. (b) t-copula model.

Fig. 8. Copula space transformation for real samples in different blocks with $p = 0.6$.

In Fig. 8(a) we plot the estimated density of the samples from the real components of subbands in two different blocks transformed to the copula space drawn from the simulated data set. We set $p = 0.6$, which means that the pair of real components do not have a sub-Gaussian α-stable distribution. We again observe the large probability mass in the corners of the figure, corresponding to strong dependence in the tails.

To verify that the dependence structure of the proposed t-copula model has the same qualitative behavior, in Fig. 8(b) we also plot the estimated density from the real components of subbands in two different blocks transformed to the copula space. In contrast with Fig. 8(a), the samples are drawn from the proposed t-copula model. As expected from the analysis of the KL divergence, the densities are very similar, again suggesting that the t-copula model fits well in this scenario.

VI. Receiver Design and Performance

In this section, we study the impact of the dependence structure on receiver performance using our tractable interference

models. We assume that a transmitter seeks to send a binary symbol $x \in \{+1, -1\}$ in the presence of interference arising from one of the scenarios detailed in Section II, with $N = 2$. Given a symbol x, the receiver observes an output $\mathbf{y} \in \mathbb{R}^K$ defined by

$$\mathbf{y} = \mathbf{g}Ax + \mathbf{z}, \tag{31}$$

where A is the transmitted signal amplitude, $\mathbf{g} \in \mathbb{R}^{2NK}$ corresponds to channel fading stacking the real and imaginary components in NK subands and $\mathbf{z} \in \mathbb{R}^{2NK}$ is interference stacking the real and imaginary components in NK subands, detailed in Section II. Each subband experiences i.i.d Rayleigh fading; i.e., $\mathbf{g} = [g_1, \cdots, g_{2NK}]$, where $g_i \sim \mathcal{N}(0, 1)$ is i.i.d. We also assume that $\mathbf{g}$ is known to the receiver, which is the common scenario where channel estimation is performed.

Given the observation $\mathbf{y}$ and equally likely symbols x, the probability of error is minimized by the likelihood ratio test

$$\Lambda(\mathbf{y}) = \frac{f(\mathbf{y}|x = 1, \mathbf{g})}{f(\mathbf{y}|x = -1, \mathbf{g})} \underset{x=-1}{\overset{x=1}{\gtrless}} 1, \tag{32}$$

where $f(\cdot|x, \mathbf{g})$ is the probability density function of the received signal given that the symbol x is transmitted and the fading is $\mathbf{g}$. As such, different receivers are obtained under the different models introduced in Sec. III. We therefore consider the following receivers:

1) Based on the t-copula α-stable model detailed in Section III-C.
2) Maximum Ratio Combining (MRC) receiver, which is optimal for Gaussian and sub-Gaussian α-stable models [24].
3) Based on the independent α-stable model [22], [23], where all components of $\mathbf{Z}$ in (5) are assumed to be independent.

To evaluate the different models in terms of the probability of error, we study the impact of the service rate (or access probability) p. Recall that the service rate is the key parameter which controls the dependence between interference on different subbands. In our study, we considered the following parameters: $\eta = 3$; $h_{j,i} \sim \mathcal{CN}(0, 1)$; $\lambda = 0.001$ devices$/m^2$; $x_{j,i}$ is uniformly drawn from $\{-1, 1\}$ $\forall i, j$; $K = 4$; and $N = 2$.

In Fig. 9, the probability of error under each of the different receivers is shown with the transmitted signal amplitude given by $A = 0.01$ based on $200,000$ Monte Carlo iterations. We first observe that when $p \to 1$, the MRC receiver outperforms other receivers due to the fact that it is optimal [24]. However, there is a negligible performance improvement over the t-copula α-stable receiver.

As $p \to 0$, the MRC receiver has poor performance. On the other hand, the t-copula α-stable receiver outperforms receivers tailored to independent α-stable noise [22], [23]. This suggests that the t-copula α-stable receiver is a tractable means of obtaining improved performance for a wide range of network parameters.

VII. Conclusions

Motivated by the challenge of interference in large-scale IoT networks exploiting NB-IoT, we have developed statistical models based on device locations modeled by general families of point processes, and copula theory. By evaluating the models in terms of the KL divergence and the probability of error when a desired link exploits non-linear combining, we have obtained significant improvements compared to standard approaches which assume independent observations on each subband. Due to the tractability of the models, it is now feasible to rapidly simulate and estimate parameters in order to improve system design.

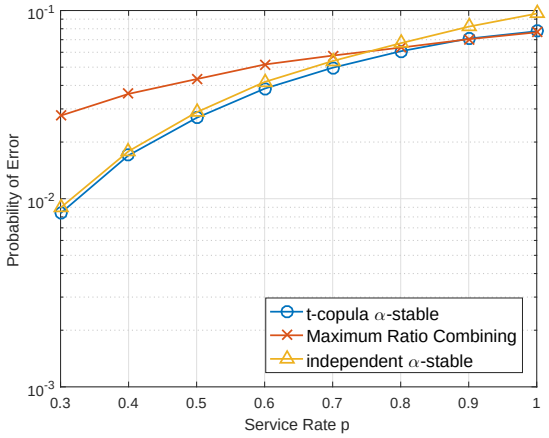

Fig. 9. Probability of error under different service rates, $\eta = 3$, $A = 0.01$ and $\lambda = 0.001$ devices$/m^2$

The key open issue is to extend the analysis to dependence in time, in addition to frequency. General models able to account for time dependence will be intimately connected to underlying queuing processes for data to be transmitted. While the results in this paper do not directly address this issue, we believe that the general techniques—including the copula methods—will provide a useful basis for further work.

Acknowledgements

This work has been (partly) funded by the French National Agency for Research (ANR) under grant ANR-16-CE25-0001 - ARBURST. It has also been supported by IRCICA, USR CNRS 3380, Lille, France and the COST Action CA15104 IRACON.

Appendix A
α-Stable Model Preliminaries

The α-stable random variables have heavy-tailed probability density functions, which have been widely used to model impulsive signals [41], [42]. The probability density function of an α-stable random variable is described by four parameters: the characteristic exponent $0 < \alpha \leq 2$; the scale parameter $\gamma \in \mathbb{R}_+$; the skew parameter $\beta \in [-1, 1]$; and the shift parameter $\delta \in \mathbb{R}$. As such, a common notation for an α-stable random variable X is $X \sim S_\alpha(\gamma, \beta, \delta)$. In the case $\beta = \delta = 0$, X is said to be a symmetric α-stable (SαS) random variable.

In general, α-stable random variables do not have closed-form probability density functions. Instead, they are usually

represented by their characteristic function, given by [42, Eq. 1.1.6]

$$\mathbb{E}\left[e^{i\theta X}\right]=\begin{cases}\exp\left\{-\gamma^{\alpha}|\theta|^{\alpha}(1-i\beta(\text{sign}\theta)\tan\frac{\pi\alpha}{2})+i\delta\theta\right\}, \alpha\neq 1\\ \exp\left\{-\gamma|\theta|(1+i\beta\frac{2}{\pi}(\text{sign}\theta)\log|\theta|)+i\delta\theta\right\}, \alpha=1\end{cases} \tag{33}$$

Let $X \sim S_{\alpha}(\sigma,\beta,\delta)$ be an α-stable random variable. A fundamental property of X is the behavior of its probability density function $p_X(x)$ as $x\to\infty$ [42, Theorem 1.2.15]

Theorem 4. *Let $X \sim S_{\alpha}(\sigma,\beta,\delta)$ with $0<\alpha<2$, then*

$$\lim_{x\to\infty} x^{\alpha}\Pr(X>x) = C_{\alpha}\frac{1+\beta}{2}\sigma^{\alpha}, \tag{34}$$

where C_{α} is defined in (8).

In the case that X is symmetric α, then $\beta=\delta=0$ and

$$\Pr(X>x) = \frac{C_{\alpha}}{2}\sigma^{\alpha}x^{-\alpha}+o(x^{-\alpha}). \tag{35}$$

An alternative characterization of symmetric α-stable random variables is the LePage series [42, Theorem 1.4.2]. In particular, let (Γ_i) denote the arrival times of a Poisson process with intensity 1. Let (W_i) be a sequence of symmetric, independent and identically distributed random variables satisfying

$$\sigma = \left(C_{\alpha}^{-1}\mathbb{E}[|W_i|^{\alpha}]\right)^{\frac{1}{\alpha}}, i=1,2,\ldots \tag{36}$$

Then,

$$X \overset{d}{=} \sum_{i=1}^{\infty}\Gamma_i^{-\frac{1}{\alpha}}W_i. \tag{37}$$

A key property of the series in (37) is given as follows.

Property 1. *Let $X \sim S_{\alpha}(\sigma,\beta,\delta)$ and $\Gamma_1^{-\frac{1}{\alpha}}W_1$ be the first term of the Lepage series in (37). Then,*

$$\lim_{x\to\infty} x^{\alpha}\Pr(X>x) = \lim_{x\to\infty} x^{\alpha}\Pr(\Gamma_1^{-\frac{1}{\alpha}}W_1>x). \tag{38}$$

Proof. According to [42, Page 26], we have

$$\Pr(\Gamma_1^{-\frac{1}{\alpha}}W_1>x) = \frac{1}{2}\mathbb{E}[|W_1|^{\alpha}]x^{-\alpha}+o(x^{-\alpha}). \tag{39}$$

Using (36), it then follows that

$$\mathbb{E}[|W_1|^{\alpha}] = C_{\alpha}\sigma^{\alpha} \tag{40}$$

and hence

$$\Pr(\Gamma_1^{-\frac{1}{\alpha}}W_1>x) = \frac{C_{\alpha}}{2}\sigma^{\alpha}x^{-\alpha}+o(x^{-\alpha}), \tag{41}$$

as required. □

It is possible to extend the notion of an α-stable random variable to the multivariate setting.

Definition 1. *A random vector $\mathbf{X}$ in $\mathbb{R}^d$ is symmetric α stable if for every $A,B>0$ there exists a $C>0$ such that*

$$A\mathbf{X}^{(1)}+B\mathbf{X}^{(2)} \overset{d}{=} C\mathbf{X}, \tag{42}$$

where $\mathbf{X}^{(1)},\mathbf{X}^{(2)}$ are independent copies of $\mathbf{X}$.

We note that each element in $\mathbf{X}$ is an α-stable random variable if $\mathbf{X}$ is an α-stable vector, but not all random vectors with symmetric α-stable marginals form symmetric α-stable random vectors.

As in the univariate case, d-dimensional symmetric α-stable random vectors are typically represented via their characteristic function, given by [42, Theorem 2.4.3]

$$\mathbb{E}\left[e^{i\boldsymbol{\theta}\cdot\mathbf{X}}\right] = \exp\left(-\int_{\mathbb{S}^{d-1}}\left|\sum_{k=1}^{d}\theta_k s_k\right|^{\alpha}\Gamma(d\mathbf{s})\right), \tag{43}$$

where Γ is the unique symmetric spectral measure on the surface of the d-dimensional unit sphere $\mathbb{S}^d$. A particular class of α-stable random vectors are an instance of the sub-Gaussian α-stable random vectors[2], defined as follows.

Definition 2. *Any vector $\mathbf{X}$ distributed as $\mathbf{X} = (A^{1/2}G_1,\ldots,A^{1/2}G_d)$, where*

$$A \sim S_{\alpha/2}((\cos\pi\alpha/4)^{2/\alpha},1,0), \tag{44}$$

and $\mathbf{G} = [G_1,\ldots,G_d]^T \sim \mathcal{N}(\mathbf{0},\sigma^2\mathbf{I})$ is called a sub-Gaussian α-stable random vector in $\mathbb{R}^d$ with underlying Gaussian vector $\mathbf{G}$.

Sub-Gaussian α-stable random vectors also play an important role in studying *complex* α-stable random variables; that is, a random variable with α-stable distributed real and imaginary components. In particular, the generalization of symmetric α-stable random variables to the complex case is known as the class of isotropic α-stable random variables, defined as follows.

Definition 3. *Let Z_1, Z_2 be two symmetric α-stable random variables. The complex α-stable random variable $Z=Z_1+iZ_2$ is isotropic if it satisfies the condition*

$$e^{i\phi}Z \overset{(d)}{=} Z \text{ for any } \phi\in[0,2\pi). \tag{45}$$

Due to the fact that baseband signals are typically complex, isotropic α-stable random variables will play an important role in the interference characterization.

The following proposition [42, Corollary 2.6.4] highlights the link between isotropic α-stable random variables and sub-Gaussian α-stable random vectors.

Proposition 1. *Let $0<\alpha<2$. A complex α-stable random variable $Z=Z_1+iZ_2$ is isotropic if and only if there are two independent and identically distributed zero-mean Gaussian random variables G_1,G_2 with variance σ^2 and a random variable $A \sim S_{\alpha/2}((\cos(\pi\alpha/4))^{2/\alpha},1,0)$ independent of $(G_1,G_2)^T$ such that $(Z_1,Z_2)^T = A^{1/2}(G_1,G_2)^T$. That is, $(Z_1,Z_2)^T$ is a sub-Gaussian α-stable random vector.*

Unlike the isotropic (or circularly symmetric) Gaussian case ($\alpha=2$), isotropic α-stable random variables with $\alpha<2$ do not have independent real and imaginary components. This dependence arises from the characterization in Proposition 1 through the dependence on the α-stable random variable A in both the real and imaginary components.

[2]There exist also sub-Gaussian α-stable random variables that allow for more general dependence structure [42], but they are not necessary for the purposes of this paper.

APPENDIX B
PROOF OF THEOREM 1

Let $N_1, N_2, \ldots$ be point processes on $\mathbb{R}^2$. Then, the sequence $(N_n)_{n=1}^{\infty}$ converges in distribution to a point process N on $\mathbb{R}^2$; i.e., $N_n \xrightarrow{d} N$ if and only if $\mathbb{E}[h(N_n)] \to \mathbb{E}[h(N)]$ for every bounded continuous function h on the space $\mathcal{N}$ of all counting measures on $\mathbb{R}^2$. Let $\mathcal{B}_N = \{B \in \mathcal{B} : N(\partial B) = 0 \ a.s.\}$ and $\mathcal{C}_c^+$ be the set of all continuous functions $f : \mathbb{R}^2 \to \mathbb{R}_+$ with compact support. Convergence in distribution is characterized in the following theorem, which will provide the link between convergence in distribution of a point process and the convergence of the interference distribution it induces.

Theorem 5 (Theorem 6.1, [43])**.** *The following statements are equivalent:*

(i) $N_n \xrightarrow{d} N$.

(ii) $\int_{\mathbb{R}^2} f(x) N_n(dx) \xrightarrow{d} \int_{\mathbb{R}^2} f(x) N(dx)$ *for all* $f \in \mathcal{C}_c^+$.

In particular, consider the interference random vector in (5). The real or imaginary component of the interference on a single subband can be written in the form

$$Z^{\kappa_n} = \sum_{j \in \Phi^{\kappa_n}_{\Gamma(r_{\min}, r_{\max})}} w_j \|\mathbf{x}_j\|^{-\eta/2}, \tag{46}$$

where $\Phi^{\kappa_n}_{\Gamma(r_{\min}, r_{\max})}$ is the point process inducing the interference and w_j represents the real or imaginary part of a term $h_{j,i}x_{j,i}$ in (4). Under the hypotheses of Theorem 1, each w_j has compact support. Let $f(\mathbf{x}, w) = w\|\mathbf{x}\|^{-\eta/2}$ which is bounded and continuous since $\Phi^{\kappa_n}_{\Gamma(r_{\min}, r_{\max})}$ and each w_j lie in compact sets. As such, we immediately obtain convergence of distribution for $\mathbf{Z}^{\kappa_n}$ as $n \to \infty$ if (i) in Theorem 5 holds.

To establish (i) in Theorem 5 holds, we require the following result.

Theorem 6 (Theorem 6.2, [43])**.** *Suppose N is simple and*

$$\lim_{m \to \infty} \limsup_{n \to \infty} P(N_n(B) > m) = 0, \ B \in \mathcal{B}. \tag{47}$$

Then, $N_n \xrightarrow{d} N$ if and only if

$$\lim_{n \to \infty} P(N_n(B) = 0) = P(N(B) = 0), \ B \in \mathcal{B}_N. \tag{48}$$

A sufficient condition for (48) to hold is given by

$$\limsup_{n \to \infty} \mathbb{E}[N_n(I)] \leq \mathbb{E}[N(I)] < \infty, \ I \in \mathcal{I}_N, \tag{49}$$

where $\mathcal{I}_N$ is the set of all intervals in $\mathcal{B}_N$.

In order to apply Theorem 6, we note that point process inducing the interference in (5) can be viewed an independently marked point process with points in $\mathbb{R}^2$ and marks in $\mathbb{C}^{KN}$, where KN is the total number of subbands. As $\Phi^{\kappa_n}_{\Gamma(r_{\min}, r_{\max})}$ is simple, the resulting marked process is simple as well.

We now establish that (49) holds for the point processes identified in Theorem 1. For the doubly Poisson cluster process, we have for all $I \in \mathcal{B}_{\Phi^{\kappa_n}_{\Gamma(r_{\min}, r_{\max})}}$,

$$\mathbb{E}\left[\Phi^{\kappa_n}_{\Gamma(r_{\min}, r_{\max})}(I)\right] = \mathbb{E}\left[\Phi^{\kappa_0}_{\Gamma(r_{\min}, r_{\max})}(I)\right] + \mathbb{E}\left[\sum_{j \in \Phi^{\kappa_0}_{\Gamma(r_{\min}, r_{\max})}} \Phi^{\kappa_n}_{d,j}(I)\right], \tag{50}$$

where $\Phi^{\kappa_n}_{d,j}$ is the daughter point process corresponding to the j-th point in $\Phi^{\kappa_0}_{\Gamma(r_{\min}, r_{\max})}$. Therefore by (49), we only need to show that

$$\limsup_{n \to \infty} \mathbb{E}\left[\sum_{j \in \Phi^{\kappa_0}_{\Gamma(r_{\min}, r_{\max})}} \Phi^{\kappa_n}_{d,j}(I)\right] = 0. \tag{51}$$

Since each $\Phi^{\kappa_n}_{d,j}$ is a homogeneous Poisson point process restricted to a particular region, it follows that the number of points in each I does not exceed that of the unrestricted homogeneous Poisson point process. Since the expected number of points for a homogeneous Poisson point process tends to zero as the intensity tends to zero, it follows that (51) holds. For the Matérn hard-core process of type II, (49) holds immediately since $\Phi^{\kappa_n}_{\Gamma(r_{\min}, r_{\max})}$ is a thinned version of $\Phi^{\kappa_0}_{\Gamma(r_{\min}, r_{\max})}$.

APPENDIX C
PROOF OF THEOREM 3

By Theorem 2, the elements of $\mathbf{Z}_b$ are $4/\eta$-stable random variables with parameter $\sigma_{\mathbf{Z}}$. Consider the first and second components of $\mathbf{Z}_{B_u}$, corresponding to the real and imaginary parts of the interference on the first subcarrier associated to block B_u. These elements can be written as

$$\begin{aligned} z_{B_{u,1}} &= \sum_{j \in \Phi_b} r_j^{-\frac{\eta}{2}} \left(\mathrm{Re}(h_{j,1})\mathrm{Re}(x_{j,1}) - \mathrm{Im}(h_{j,1})\mathrm{Im}(x_{j,1})\right) \\ z_{B_{u,2}} &= \sum_{j \in \Phi_b} r_j^{-\frac{\eta}{2}} \left(\mathrm{Re}(h_{j,1})\mathrm{Im}(x_{j,1}) + \mathrm{Im}(h_{j,1})\mathrm{Re}(x_{j,1})\right). \end{aligned} \tag{52}$$

Assume that $h_{j,1} \sim \mathcal{CN}(0,1)$ (a similar argument holds for the case of Gaussian inputs). Consider the random vector $\mathbf{Z}^l_{B_u}$, corresponding to the contribution of device $l \in \Phi_b$ on each subcarrier associated to block B_u. This can be written as

$$\mathbf{Z}^l_{B_u} = r_l^{-\eta/2} \left(\mathbf{f} \odot \mathrm{Re}(x_l) + \mathbf{g} \odot \mathrm{Im}(x_l)\right), \tag{53}$$

where $\odot$ is the Hadamard (element-wise) product. Since $h_{i,j} \sim \mathcal{CN}(0,1)$, it follows that $\mathbf{f}$ and $\mathbf{g}$ are Gaussian random vectors with independent components with the same variance. It then follows that for any orthogonal matrix $\mathbf{U}$ in the set of real orthogonal matrices $\mathcal{O}(2N)$ of dimension $2N \times 2N$,

$$\mathbf{U}\mathbf{f} \overset{d}{=} \mathbf{f}, \quad \mathbf{U}\mathbf{g} \overset{d}{=} \mathbf{g}. \tag{54}$$

This in turn implies that $\mathbf{U}\mathbf{Z}^l_b \overset{d}{=} \mathbf{Z}^l_b$ and hence $\mathbf{U}\mathbf{Z}_b \overset{d}{=} \mathbf{Z}_b$.

To complete the proof, we apply the following lemma which is a straightforward generalization of [42, Theorem 2.6.3].

Lemma 1. *Let $\mathcal{O}(d)$ be the set of real orthogonal matrices and $\mathbf{U} \in \mathcal{O}(d)$. Let $\mathbf{Z}$ be an α-stable random vector on $\mathbb{R}^d$. Then, $\mathbf{Z} \overset{d}{=} \mathbf{U}\mathbf{Z}$ if and only if $\mathbf{Z}$ is a sub-Gaussian α-stable random vector with an underlying Gaussian vector having i.i.d. $\mathcal{N}(0, \sigma^2)$ components.*

REFERENCES

[1] C. Zheng, M. Egan, L. Clavier, G. Peters, and J.-M. Gorce, "Copula-based interference models for iot wireless networks," in *ICC 2019-53rd IEEE International Conference on Communications*, pp. 1–6, 2019.

[2] Y. D. Beyene, R. Jantti, O. Tirkkonen, K. Ruttik, S. Iraji, A. Larmo, T. Tirronen, and J. Torsner, "Nb-iot technology overview and experience from cloud-ran implementation," *IEEE Wireless Communications*, vol. 24, pp. 26–32, Jun. 2017.

[3] A. Hoglund *et al.*, "Overview of 3GPP release 14 enhanced NB-IoT," *IEEE Network*, vol. 31, pp. 16–22, Dec. 2017.

[4] J. Schlienz and D. Raddino, "Narrowband Internet of Things whitepaper," *IEEE Microw. Mag.*, vol. 8, pp. 76–82, Aug. 2016.

[5] E. Sousa, "Performance of a spread spectrum packet radio network link in a Poisson field of interferers," *IEEE Transactions on Information Theory*, vol. 38, no. 6, pp. 1743–1754, 1992.

[6] J. Ilow and D. Hatzinakos, "Analytic alpha-stable noise modeling in a poisson field of interfers or scatterers," *IEEE Transactions on Signal Processing*, vol. 46, no. 6, pp. 1601–1611, 1998.

[7] P. Pinto and M. Win, "Communication in a Poisson field of interferers-part I: interference distribution and error probability," *IEEE Transactions on Wireless Communications*, vol. 9, no. 7, pp. 2176–2186, 2010.

[8] P. Pinto and M. Win, "Communication in a Poisson field of interferers-part II: channel capacity and interference spectrum," *IEEE Transactions on Wireless Communications*, vol. 9, no. 7, pp. 2187–2195, 2010.

[9] K. Gulati, B. Evans, J. Andrews, and K. Tinsley, "Statistics of co-channel interference in a field of Poisson-Poisson clustered interferers," *IEEE Transactions on Signal Processing*, vol. 58, no. 12, pp. 6207–6222, 2010.

[10] C. Zheng, M. Egan, L. Clavier, G. Peters, and J.-M. Gorce, "On the validity of isotropic complex α-stable interference models for interference in the iot," 2019.

[11] M. Lauridsen, B. Vejlgaard, I. Kovács, H. Nguyen, and P. Mogensen, "Interference measurements in the European 868 MHz ISM band with focus on LoRa and SigFox," in *IEEE Wireless Communications and Networking Conference (WCNC)*, 2017.

[12] B. Vejlgaard, M. Lauridsen, H. Nguyen, I. Z. Kovács, P. Mogensen, and M. Sorensen, "Interference impact on coverage and capacity for low power wide area iot networks," in *2017 IEEE Wireless Communications and Networking Conference (WCNC)*, pp. 1–6, IEEE, 2017.

[13] L. Clavier, T. Pedersen, I. Rodriguez, M. Lauridsen, and M. Egan, "Experimental evidence for heavy tailed interference in the IoT." Preprint available https://hal.archives-ouvertes.fr/hal-02521928, 2020.

[14] J. Andrews, F. Baccelli, and R. Ganti, "A tractable approach to coverage and rate in cellular networks," *IEEE Transactions on Communications*, vol. 59, no. 11, pp. 3122–3134, 2011.

[15] H. ElSawy, A. Sultan-Salem, M. Alouini, and M. Win, "Modeling and analysis of cellular networks using stochastic geometry: a tutorial," *IEEE Communications Surveys & Tutorials*, vol. 19, no. 1, pp. 167–203, 2017.

[16] M. Haenggi and R. Ganti, "Interference in large wireless networks," *Foundations and Trends in Networking*, vol. 3, no. 2, pp. 127–248, 2009.

[17] M. Egan, M. de Freitas, L. Clavier, A. Goupil, G. Peters, and N. Azzaoui, "Achievable rates for additive isotropic alpha-stable noise channels," in *Proc. of the IEEE International Symposium on Information Theory*, 2016.

[18] M. Egan, L. Clavier, M. de Freitas, L. Dorville, J.-M. Gorce, and A. Savard, "Wireless communication in dynamic interference," in *IEEE Global Communications Conference (GLOBECOM)*, 2017.

[19] M. de Freitas, M. Egan, L. Clavier, G. Peters, and N. Azzaoui, "Capacity bounds for additive symmetric alpha-stable noise channels," *IEEE Transactions on Information Theory*, vol. 63, pp. 5115–5123, Aug. 2017.

[20] J. Fahs and I. Abou-Faycal, "On properties of the support of capacity-achieving distributions for additive noise channel models with input cost constraints," *IEEE Transactions on Information Theory*, vol. 64, pp. 1178–1198, Feb. 2018.

[21] M. Freitas, M. Egan, L. Clavier, A. Savard, and J.-M. Gorce, "Power control in parallel symmetric α-stable noise channels," *preprint, available:*, 2018.

[22] S. Niranjayan and N. Beaulieu, "The BER optimal linear rake receiver for signal detection in symmetric alpha-stable noise," *IEEE Transactions on Communications*, vol. 57, pp. 3585–3588, Dec. 2009.

[23] S. Niranjayan and N. Beaulieu, "BER optimal linear combiner for signal detection in symmetric alpha-stable noise: small values of alpha," *IEEE Transactions on Wireless Communications*, vol. 9, pp. 886–890, Mar. 2010.

[24] C. Zheng, M. Egan, T. Pedersen, and J.-M. Gorce, "Linear combining in dependent α-stable interference," in *Proc. IEEE International Conference on Communications (ICC)*, 2020.

[25] H. Nikopour and H. Baligh, "Sparse code multiple access," in *IEEE International Symposium on Personal Indoor and Mobile Radio Communications (PIMRC)*, 2013.

[26] F. Baccelli, B. Blaszczyszyn, and P. Muhlethaler, "An aloha protocol for multihop mobile wireless networks," *IEEE Transactions on Information Theory*, vol. 52, no. 2, pp. 421–436, 2006.

[27] M. Haenggi, *Stochastic Geometry for Wireless Networks*. New York, NY: Cambridge University Press, 2013.

[28] M. Egan, L. Clavier, C. Zheng, M. de Freitas, and J.-M. Gorce, "Dynamic interference for uplink SCMA in large-scale wireless networks without coordination," *EURASIP Journal on Wireless Communications and Networking*, vol. 1, 2018.

[29] R. Nelson, *An Introduction to Copulas*. New York, NY: Springer-Verlag, 1999.

[30] S. Demarta and A. McNeil, "The t-copula and related copulas," *International Statistical Review*, vol. 73, no. 1, pp. 111–129, 2005.

[31] F. Lindskog, A. Mcneil, and U. Schmock, "Kendall's elliptical distribution rope," in *Credit Risk*, pp. 149–156, Springer, 2003.

[32] P. Rousseeuw and G. Molenberghs, "Transformation of non positive definite semidefinite correlation matrices," *Comm. Statist. Theory Methods*, vol. 22, pp. 965–984, 1993.

[33] S. Kring, S. T. Rachev, M. Höchstötter, and F. J. Fabozzi, "Estimation of α-stable sub-gaussian distributions for asset returns," in *Risk Assessment*, pp. 111–152, Springer, 2009.

[34] "Alpha-stable distributions in matlab." http://math.bu.edu/people/mveillet/html/alphastablepub.html.

[35] "Copulafit." https://www.mathworks.com/help/stats/copulafit.html.

[36] Q. Wang, S. R. Kulkarni, and S. Verdú, "A nearest-neighbor approach to estimating divergence between continuous random vectors," in *2006 IEEE International Symposium on Information Theory*, pp. 242–246, IEEE, 2006.

[37] Z. Szabó, "Information theoretical estimators toolbox," *Journal of Machine Learning Research*, vol. 15, pp. 283–287, 2014.

[38] B. Cho, K. Koufos, and R. Jantti, "Bounding the mean interference in matérn type ii hard-core wireless networks," *IEEE wireless communications letters*, vol. 2, no. 5, pp. 563–566, 2013.

[39] M. Haenggi, "Mean interference in hard-core wireless networks," *IEEE Communications Letters*, vol. 15, no. 8, pp. 792–794, 2011.

[40] A. M. Ibrahim, T. ElBatt, and A. El-Keyi, "Coverage probability analysis for wireless networks using repulsive point processes," in *2013 IEEE 24th Annual International Symposium on Personal, Indoor, and Mobile Radio Communications (PIMRC)*, pp. 1002–1007, IEEE, 2013.

[41] C. Nikias and M. Shao, *Signal processing with alpha-stable distributions and applications*. New York, NY: Wiley, 1995.

[42] G. Samorodnitsky and M. Taqqu, *Stable Non-Gaussian Random Processes*. New York, NY: CRC Press, 1994.

[43] R. Serfozo, "Point processes," in *Handbooks in Operations Research and Management Science Volume 2* (D. Heyman and M. Sobel, eds.), ch. 1, pp. 1–93, North-Holland: Elsevier Science Publishers B.V., 1990.